Recent ASDEX Upgrade results and future extension plans

A. Kallenbach*, V. Bobkov*, F. Braun* A. Herrmann*, H. Höhnle†, R.M. McDermott*, R. Neu*, J.-M. Noterdaeme*, T. Pütterich*, J. Schweinzer*, J. Stober*, E. Strumberger*, W. Suttrop*, D. Wagner*, H. Zohm*, ASDEX Upgrade Team *Max-Planck-Institut für Plasmaphysik, Association EURATOM-IPP, D-85748 Garching, Germany
Email: Arne.Kallenbach@ipp.mpg.de
†Institut f. Plasmaforschung, Universität Stuttgart, D-70569 Stuttgart, Germany

***Abstract*—ASDEX Upgrade is an ITER shaped divertor tokamak with versatile heating, fueling, exhaust and control systems. All plasma facing components are coated with tungsten layers. Plasma scenarios have been adopted that avoid central tungsten accumulation, which can lead to an H-L transition due to excessive central radiative losses. Compared to a carbon-PFC tokamak, the AUG operational space is slightly more weighted towards higher densities and collisionalities. Actual and future planned extensions aim towards reducing the core collisionality while maintaining good power and particle exhaust. These extensions include a solid tungsten outer divertor target, improved pumping, higher ECRH power and modified ICRF antennas that reduce tungsten sources. The newest element for advanced plasma control is the first set of 8 magnetic perturbation coils, which already achieved type-I ELM mitigation in multiple plasma scenarios. Another 8 coils have been installed in autumn 2011 allowing the production of mode spectra with n $>$ 2. In parallel to the improved actuator set, an increasing number of diagnostics are brought into real-time state, allowing versatile profile and stability control.**

***Index Terms*—Fusion devices, ECRH, ICRF, divertor, plasma facing components, tungsten**

I. Introduction

ASDEX Upgrade (AUG) is an ITER-like tokamak with about 1/4 of its linear dimensions [1]. The poloidal field coil system is mounted outside the toroidal field coils, making shaping and plasma control more demanding compared to machines with shaping coils close to the plasma. Since 2007, all plasma facing components are coated with tungsten [2], see figure 1. The experimental requirement to avoid tungsten accumulation results in the AUG typical operational domain being situated at higher collisionalities compared to similar sized carbon devices [3] [4]. Feedback controlled radiative cooling using nitrogen has become an integral element of high heating power scenarios to avoid target power overload [5].

The main actuators used to achieve low core tungsten concentrations are central wave heating and deuterium gas puffing, the latter mainly acting via an increased edge localised mode (ELM) frequency resulting in pedestal impurity flushing [6] [7].
The most recent plasma control tool is ELM mitigation by magnetic perturbation coils, where the first set of 8 coils was installed and commissioned in 2010 [8]. Future planned extensions aim towards increased central heating capabilities and higher divertor peak power loads, both of which allow the extention of the operational space towards lower collisionalities. These extensions should also result in a gain in performance as well as an improved capability for local plasma control. Along these lines, the planned future extensions of ASDEX Upgrade are motivated by the results achieved with the recent upgrades in the 2010/11 experimental campaign. These are comprised of 2 additional long-pulse, double frequency (105 and 140 GHz) gyrotrons, an ICRF antenna with reduced tungsten release, an upgrade of the outer divertor with solid tungsten tiles and an increasingly versatile system of magnetic perturbation coils.

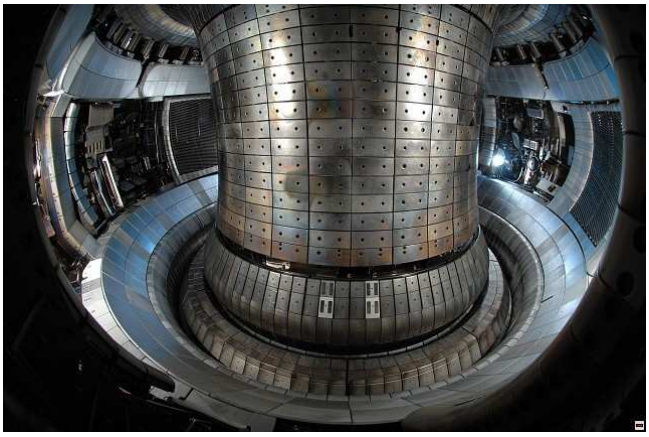

Fig. 1. AUG in vessel view autumn 2010 with fully tungsten coated plasma facing components.

II. Divertor development

ASDEX Upgrade has undergone a series of divertor modifications which are shown in figure 2. The present divertor version is Div IId. Versions IIb and IIc are not shown since their large scale shapes differ only slightly from version IId. The original divertor configuration Div I, which is still present in the upper divertor, is a quite open configuration with approximately horizontal plates situated in the high flux expansion region close to the X-point. Divertor II was changed into a vertical configuration with originally highly shaped surfaces to obtain relatively flat field line impact for optimised power load. Div II has also been equipped with a roof baffle for better neutral compression and a cryopump which added

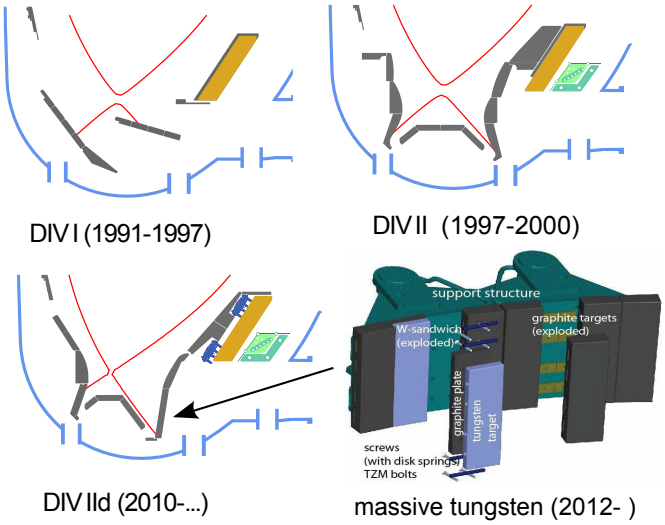

Fig. 2. Development of ASDEX Upgrade divertor design versions. The next scheduled modification is the exchange of the tungsten-coated tiles of the current Div IId with solid tungsten tiles, labeled Div III.

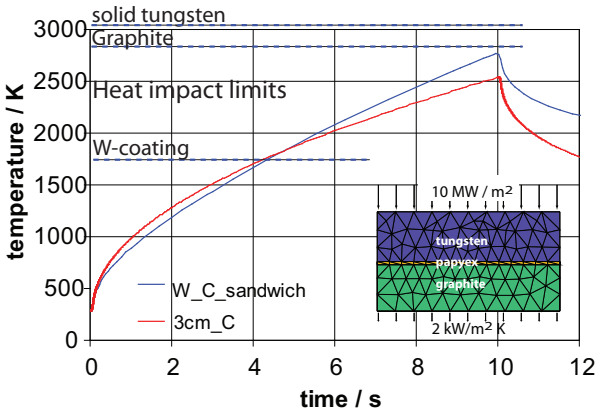

Fig. 3. FEM calculation of the impact of a 10 MW/m^2 perpendicular heat flux on a tungsten/carbon sandwich tile for the solid tungsten divertor III. Surface temperatures for a 10 s heating interval are shown for the W/C sandwich compared to a graphite tile. The maximum acceptable surface temperature for tungsten, graphite and tungsten coatings are also shown.

to the pumping speed of the turbomolecular pumps (13 m$^3/s$) another 100 m$^3/s$. In the subsequent divertor modification to Div IIb, the detailed poloidal shaping of the surface was relaxed and the roof baffle was shortened to allow more flexible plasma shaping, in particular with higher triangularity. The more shallow angles of incidence introduced with Div II were given up with Div IIb, changing to simpler, flat target plates. Ordinary fine grain graphite was chosen for the outer strike point region instead of the carbon-fibre-reinforced carbon (CFC) used in Div II. Tile edge shadowing by roof-like tilting and polygonal shaping are used to avoid thermal overload on leading edges. No significant degradation of neutral compression or power exhaust behaviour was observed in the modfication to Div IIb [9]. With Div IIc, 200 μm thick vaccum plasma sprayed (VPS) tungsten coatings were introduced on divertor PFCs. Due to delamination events under high heat fluxes, the thick VPS coatings were replaced by tiles with thin ($\approx$ 10 μm) CSMII coatings [10]. The next AUG divertor modification (Div III) will be the change of the outer vertical target to solid tungsten PFCs, scheduled for installation in autumn 2012 [11]. The solid tiles will feature a sandwich structure with graphite plates attached below the solid tungsten plates for weight reduction, see figure 2. This will allow for higher surface temperatures and overcome the limitations of tungsten coatings, resulting in a better power handling capability, as shown in figure 3. Some of the solid tiles may also get castellations grooved in, to test the impact of heat loads on such structures and to measure fuel retention by co-deposition in small gaps. In parallel, the neutral conduction from the divertor to the pumping chamber will be increased to obtain a higher effective pumping speed.

III. Heating and Current Drive Systems

A. Neutral beam injection

AUG is equipped with 2 neutral beam injection (NBI) boxes each with 4 sources and a total of 10 MW heating power. Box I has 60 kV, box II 93 kV ion acceleration voltage. The power of a source can be reduced by decreasing the voltage or by beam modulation. The voltage reduction is also used to shift the deposition range further outside. Two sources of injector box II have been tilted to provide off-axis current drive in the co-current direction [12]. While the total driven current could be verified, a radial de-localization of the driven current at high total heating powers was observed [13]. Whether this effect is due to anomalous fast ion transport is currently under investigation using the new fast ion D$_\alpha$ (FIDA) diagnostic [14]. The NBI system provides the basic heating used in the majority of AUG discharges. After upgrading the charge exchange recombination spectroscopy (CXRS) diagnostic, short beam blips (of the order of 10 msec duration) are used for diagnostic purposes in ECRH or ICRF heated discharges for ion temperature and rotation measurements with only small plasma perturbation.

B. ICRF status and extensions

The ICRF system has four 2-strap antennas (see figure 4 left), connected as 2 pairs to the HF generators with 3dB couplers allowing good power coupling under ELMy H-mode conditions. Since ICRF operation has been found to cause strong tungsten influx from neighboring limiters [15], its use has been restricted to high density scenarios or limited power in the all-tungsten clad AUG. Figure 4 shows an experiment where two antenna pairs were powered alternately [16]. Powering antennas 3+4 (first and third pulse), a current is measured to flow into the corresponding antenna frame which indicates a modified sheath potential caused by the antenna action. Powering antennas 1+2 (middle pulse), a rectified positive plasma potential of the order of 100 V is measured by a floating probe tip in a position 4 m away, but magnetically connected to the antenna 1+2 pair vicinity. The spectroscopic measurements on the limiters of antennas 3+4 reveal a drastically increased tungsten sputtering yield while powered (lowest graph). The signals shown suggest the occurence of a rectified sheath potential caused by the ICRF

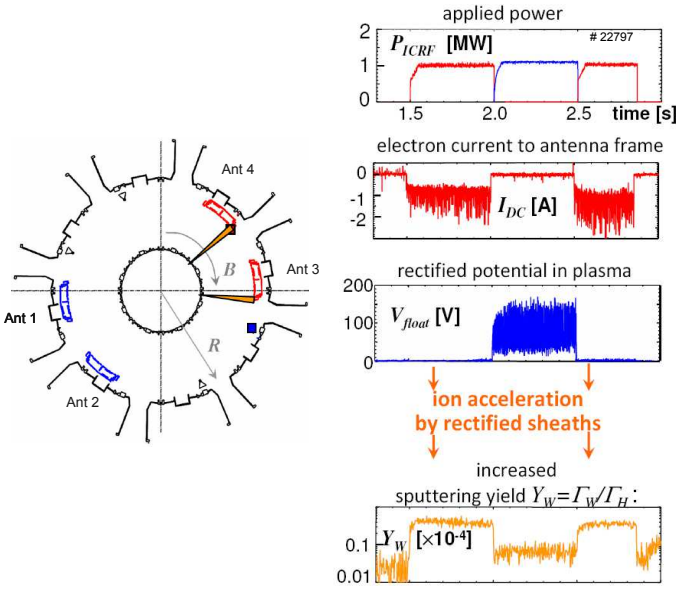

Fig. 4. left: Positions of the ICRF antennas and antenna limiter spectroscopic observations in the AUG torus. right: measurement of sheath voltage and corresponding rise in tungsten erosion yield.

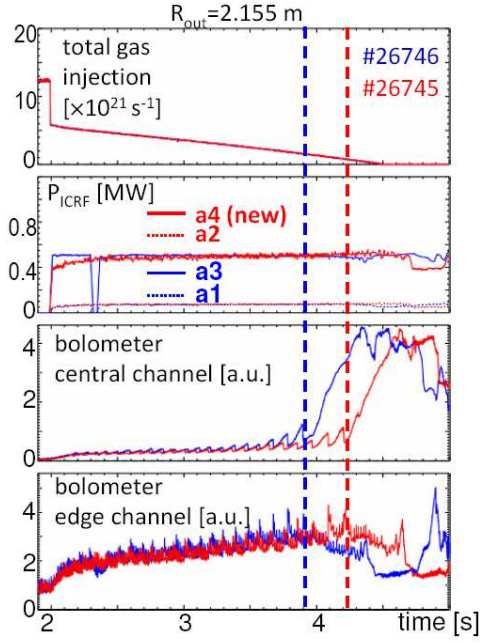

Fig. 5. Comparison of tungsten accumulation behaviour using the old (blue) and the new, broadened (red) ICRF antennas. The occurrence of accumulation at a lower gas puff level indicates a better ratio of central heating to tungsten source.

operation, which leads to plasma and impurity ion acceleration to the antenna limiters causing enhanced tungsten sputtering.

Currently, an improved antenna design is being developed with the aim to reduce the W source during ICRF operation. An important ingredient is the reduction of mirror currents in the antenna box, which contribute significantly to the near field causing the W influx. In the previous vent, ICRF antenna 4 was modified and equipped with broader limiters in order to reduce the tungsten source and to validate the code

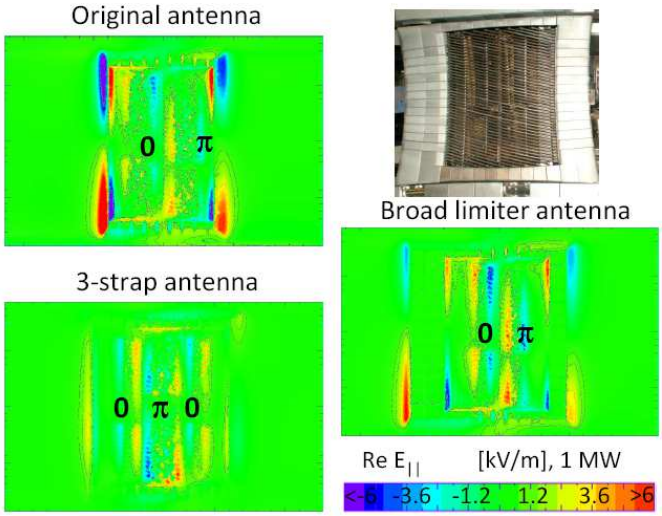

Fig. 6. HFSS code calculations of antennas near E-fields which are supposed to cause the W-source at the ICRF limiters.

calculations which highlight the importance of the antenna box mirror current. Figure 5 compares the W accumulation behaviour of this modified antenna with the old design. The W accumulation onset is taken as a measure for the balance of central heating and connected additional tungsten source. Ramp-down of the deuterium gas puff (see upper graph of figure 5) was used, since the minimum deuterium puff required to avoid W accumulation was previously found to be a good figure of merit for W-compatibility of a heating scenario [16]. The tungsten accumulation with the modified antenna occurs reproducibly later, pointing to a moderate improvement of its W-compatibility. Further antenna development seeks for a higher degree of improvement, with the final goal to make ICRF fully high-Z compatible. The favourite future antenna design candidate is currently a 3-strap antenna, with the current in the central strap being about 2 times higher compared to each of the side straps, allowing for a compensation of the mirror currents caused by central and side straps. Figure 6 shows calculations of the antenna near fields for the old design, the modified broad antenna and a possible 3-strap antenna. Development and installation of the new antennas is foreseen to follow a step-wise approach, with subsequent validations of the antenna modelling predictions. The final antenna set will be integrated into a possible conductive wall design in 2015 or later.

C. ECRH status and extensions

The ECRH system comprises currently two systems. The old ECRH I system consists of four 140 GHz, 0.5 MW gyrotrons with 2 s pulse length. The new ECRH II system has 3 two-frequency (105 and 140 GHz), 10 s gyrotrons with up to 1 MW each, a fourth gyrotron is expected to be installed in spring 2012. Different ECRH heating and current drive scenarios have been developed. In addition to the standard X2-mode, O2 heating has been developed to avoid the cutoff at high densities ($n_{e,cutoff}(X2)$= 1.22 10^{20} m^{-3} for B_t= 2.5 T, f= 140 GHz, T_e= 2 keV). To overcome the low single-

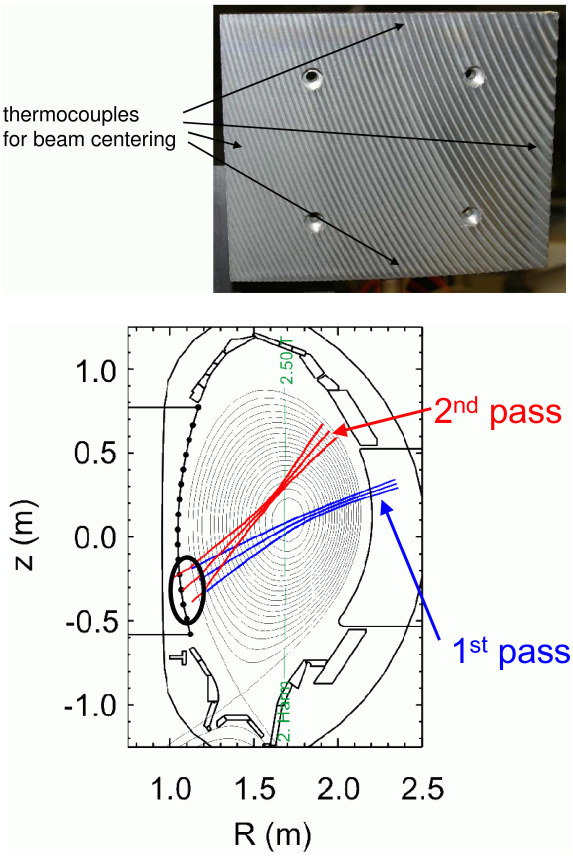

Fig. 7. Arrangement for reflection of ECRH shine-through on the high field side to improve absorption of O2 heating.

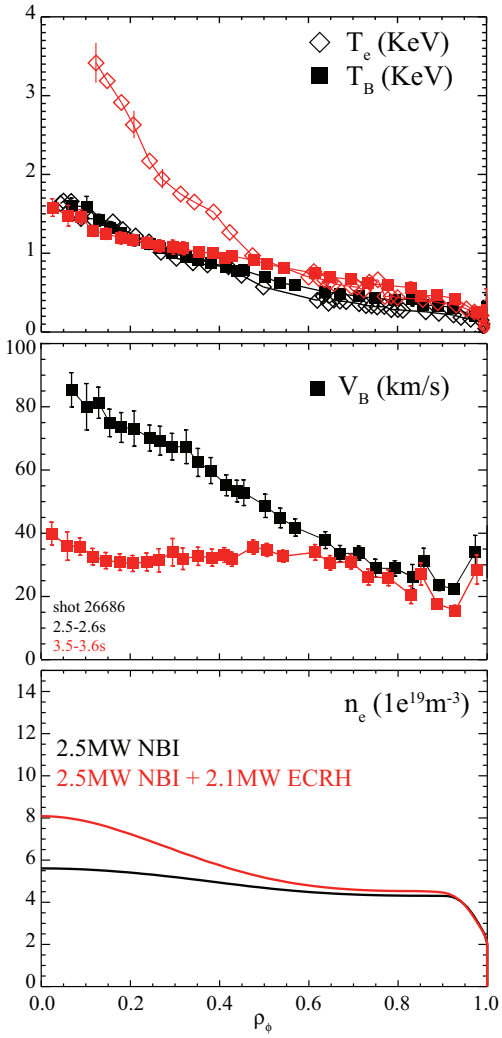

Fig. 8. Comparison of plasma profiles in a NBI-heated H-mode discharge with and without additional ECRH. Shown are the electron and the (boron) ion temperature, the toroidal rotation velocity and the electron density. Plasma current I_p= 0.6 MA, toroidal field B_t= 2.5 T.

path absorption of ≈ 70-80 % of the O2-mode, two tiles of the inner wall have been replaced with holographic focusing mirrors, allowing an increase in the absorption of up to 90 %. Figure 7 shows a reflector and the typical ECRH beam path for the O2-scheme. X3-heating with f= 140 GHz at B_t=1.8 T is used for scenarios with reduced safety factor q_{95}= 3 at I_p = 1.1 MA. Here, the X2 resonance at the high field side pedestal top acts as a beam dump for the X3 shine through. Finally, the ITER like O1 scheme has also been successfully tested at AUG with B_t= 3.2 T and 105 GHz gyrotron frequency.

The newly upgraded ECRH capability has been used for central heating for tungsten accumulation avoidance, dedicated transport studies and MHD control. Transport studies take advantage of the exclusive heating of the electrons by ECRH. Of particular interest are scans of the T_e/T_i in the transition region between dominant ion temperature gradient driven (ITG) modes and trapped electron modes (TEM), where pronounced changes of the electron density profile peaking as a result of ECRH are observed [17] and reproduced by theoretical predictions [18]. An example of such drastic changes of the profile shapes due to ECRH is shown in figure 8 [19]. The centrally deposited ECRH causes a strong rise of the central electron temperature, decoupling it from the ion temperature, a pronounced reduction of the central toroidal rotation and a peaking of the electron density profile. The peaking of the density profile with ECRH in this low plasma current discharge is opposite to what is usually observed with higher currents. This is explained by the plasma transport being dominated by TEM rather than by ITG modes [18]. AUG discharges with higher plasma current and higher density are typically ITG dominated, and central ECRH leads to a flattening of the electron density profile. This effect is also used for real-time feedback control of the electron density profile in AUG [20].

Another interesting feature of ECRH is the fact that there is no direct momentum input allowing, in the combination with neutral beam heating, an independent variation of heat flux and momentum flux. Spontaneous plasma rotation without direct momentum input has been found to exhibit a rich phenomenology in Alcator C-Mod [21]. Figure 9 shows radial profiles of the toroidal plasma rotation in AUG with varying heating power and no external momentum sources, using short NBI beam blips for the CXRS diagnostic. The first spectrum taken during the blip can be regarded as unperturbed by the beam momentum in good approximation [19]. For the present conditions, the central plasma rotates in the counter current (negative) direction, while the edge rotates co-current. The central rotation gets more negative with increasing heating

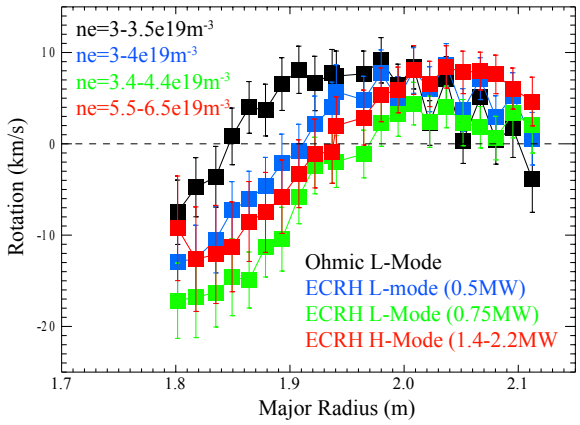

Fig. 9. Profiles of toroidal plasma rotation for discharges without external momentum input measured with CXRS using NBI blips.

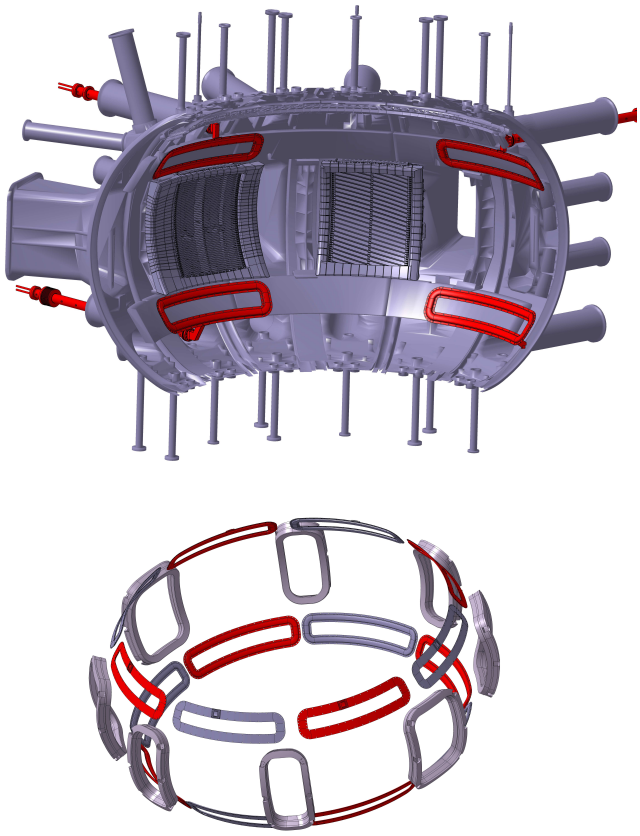

Fig. 10. Current installation of 8 magnetic perturbation coils and planned final setup after the next 2 stages.

power in L-mode. In H-mode, at higher ECRH power, a positive offset velocity shifts the profile towards the co-current direction.

The combination of central heating by ECRH and simultaneous active control of neoclassical tearing modes (NTM) is planned for the near future [22]. Provided sufficient financial resources, exchange of the old ECRH I gyrotrons by high-power, long pulse gyrotrons is planned, and will be named ECRH III. This extension could be finished in 2016 and result in up to 6.5 MW deposited ECRH power for 10 s pulse length and 2-frequency step-tunability.

IV. ELM CONTROL WITH MAGNETIC PERTURBATIONS

The first set of 8 magnetic perturbation (MP) coils (named B-coils) was installed in 2010 with the major aim to obtain mitigation of type-I ELMs [23] [24]. The arrangement of the coils in the torus is shown in figure 10. Experiments on ELM mitigation were performed for various plasma scenarios and heating mixes [8]. Figure 11 shows an example for such an experiment. About 200 ms after switching on the MP coils, the large type-I ELMs completely vanish, they reappear soon after coil switch-off. During the phase without type-I ELMs small, periodic, high frequency burst-like events appear with one fifth or less of a type-I ELM power amplitude. They are best resolved in the pedestal electron temperature measured by electron cyclotron emission (ECE) shown in figure 11. Time dependent power load profiles from the inner and outer divertor are shown in figure 12. During the mitigated phase, strike point splitting in the outer divertor can be clearly seen. The splitting is compatible with field line tracing calculations without screening of the perturbation. The power load in the outer divertor rises slightly during the MP phase, which may be explained by the omission of the power flux carried by type-I ELMs. No density or energy pumpout is observed for standard H-mode plasma conditions.

ELM mitigation is obtained with the magnetic perturbation coils in AUG above a critical pedestal density, which scales approximately linearly with the plasma current. Other parameters like heating power, plasma rotation and safety factor appear to be of minor importance. Surprisingly, the magnetic configuration of the coils (resonant or non-resonant) is also not important. Although strike point splitting in the divertor is observed during ELM mitigation, the magnetic perturbations seem to be screened by the bulk plasma, since no change of rotation has been observed during MP experiments so far. Because the critical density lies in the medium-high density H-mode operational space, first experiments with pellets combined with MP were performed. During the ELM mitigated phase, the pellets led to a density increase, but did not trigger ELMs. The tungsten content of the main plasma does not increase during the ELM mitigated phase, often even a moderate reduction is observed. This suggests that the prevailing small, burst-like events are efficient enough to flush out tungsten from the pedestal region.

So far, no theoretical explanation for the ELM mitigation mechanisms in ASDEX Upgrade exists. In particular, the lack of influence of both the MP on the plasma rotation as well as the edge rotation on the ELM mitigation effect are surprising. Further experiments are required and foreseen to disentangle the response of the plasma edge to the applied perturbations. As the next extension of the AUG magnetic perturbation coils system, another 8 B-coils have just been installed above and below the midplane, resulting in full toroidal coverage with 16 coils in total. These will enable a more flexible mode spectrum, like n=4. Further on, AC-amplifiers are foreseen for studies with rotating fields, which can be used with frequencies up to about 800 Hz for the present B-coils. The MP coil scheme will be accomplished around 2015/16 by another set of 8 'A-

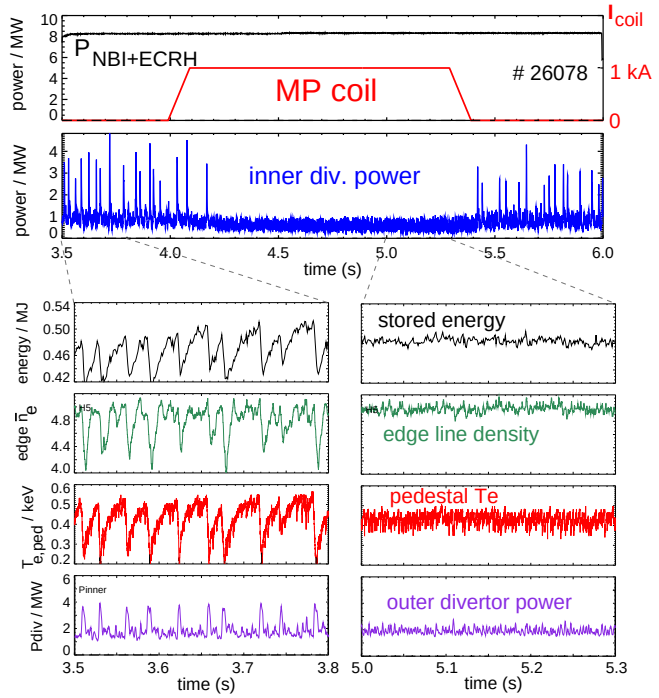

Fig. 11. Time traces of a discharge with and without ELM mitigation by magnetic perturbation. The upper graph shows the heating power and the current in the MP coil, as well as the power in the inner divertor highlighting the phase with type-I ELM mitigation. The lower graphs compare plasma parameters before and during ELM mitigation.

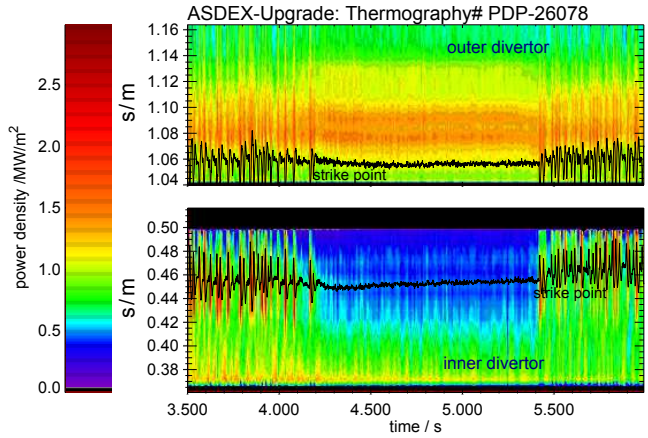

Fig. 12. Time dependent 1D-distribution of the divertor heat load in inner and outer divertor for the discharge of figure 11 measured by infra-red thermography. Strike-point splitting at the outer target is clearly visible during the ELM mitigation phase.

coils', which will be positioned in the midplane around the large A-ports. These coils can handle AC frequencies up to 3 kHz and will be used for various MHD studies, including resistive wall mode control.

V. Scenario Development for Integrated Power Exhaust Control

With the finalization of the ITER design, the ASDEX Upgrade programme develops a new focus on ITER operation and DEMO studies. High power exhaust studies, integrated with real-time control of various parameters, is one

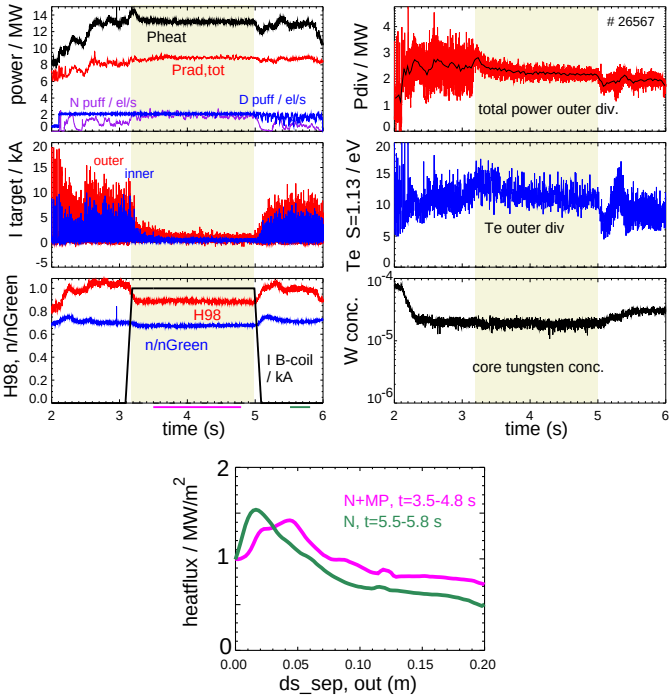

Fig. 13. Time traces of a discharge with combined feedback controlled nitrogen seeding and ELM mitigation by magnetic perturbations with n=2, odd parity. The lower graph shows heat flux profiles along the outer target during N seeding and N seeding combined with ELM mitigation by MPs.

key element. Figure 13 shows a discharge which combines feedback-control of the divertor heatflux by nitrogen seeding and ELM mitigation by magnetic perturbations at 14 MW heating power. Under these conditions moderate energy and density pumpout are observed, approximately retracting the improvement caused by the N seeding. The already quite small ELMs due to N seeding [5] are even further reduced in size by the additional MP action, resulting in ELM energies below 10 kJ. As a result of the N seeding, the time averaged peak heat flux in the outer divertor stays around 1.5 MW/m^2. For a future ITER or DEMO, control of only one radiating species will not be sufficient. Simultaneous and independent control of the target heat flux/divertor radiation and the core radiation will be required to dissipate the enormous power flux, which may be a factor of 5 higher in DEMO compared to ITER [25]. First experiments with 2 seeding species (N, Ar) were started in AUG. The core radiation was increased by a pre-programmed Ar puff while the divertor heat flux was feedback-controlled with nitrogen seeding. [26]. The reduction of the core heat flux by a medium-Z radiator leads to a decreased type-I ELM frequency, which may become too low to prevent central W accumulation in the all-tungsten AUG. Therefore, combination with ELM control is essential. Corresponding experiments are planned for the near future, implementation of a double-feedback for core radiation and divertor heat load are planned for the 2012.

VI. Summary and Extension Schedule

The AUG extension schedule is shown in figure 14. The schedule reflects the actual construction and financial plan,

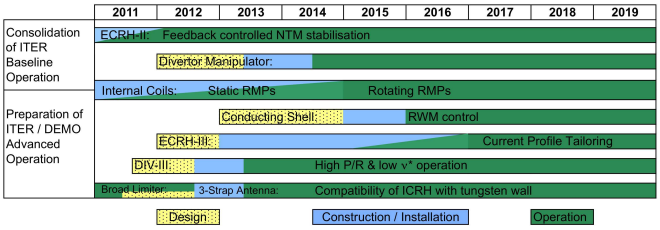

Fig. 14. Gantt chart of the AUG extension planning.

which may be subject to changes in the future. The next set of eight MP coils has recently been mounted and is ready for the 2012 experimental campaign. Solid tungsten tiles foreseen for the Divertor III upgrade which is scheduled for winter 2012 have been successully tested in IPP's GLADIS high heat flux facility, two tests tiles are installed in the AUG divertor in the current campaign. Divertor III will also be equipped with a larger version of the current divertor manipulator, allowing in-situ tests of complete high heat flux components or to investigate operation with damaged tungsten divertor tiles as requested by ITER. The ECRH III extension which could be completed in 2016 will lead to a total gyrotron power of 8 MW and about 6.5 MW deposited in the plasma. It will facilitate strong electron heating and provide the flexibility to combine tasks like power modulation experiments, active NTM stabilisation, current profile tailoring and tungsten accumulation prevention. The final part of the mid-term extensions is the implementation of a conducting wall, as shown in figure 15. Its realisation will depend on the occurence of resistive wall modes (RWM) in ASDEX Upgrade, which may itself depend on the current drive capabilities. Also shown are RWM growth rates for different wall coverage schemes. The RWM stability can be increased up to $\approx$ 50 % in advanced scenarios, the best values are expected if the Faraday screens of the ICRF antennas are connected to the conducting wall. In addition to the two 'current drive' beams of neutral beam box II which are focused at mid-radius, the ECRH system with its fully steerable launchers has current drive capability, albeit with moderate efficiency and preferably at high electron temperatures. The ECRH III extension will improve the current profile tailoring ability in particular in the central plasma region. For current drive in the outer plasma region, a lower hybrid (LH) system has also been considered. Plans for installation of such a system have been put aside for financial and manpower reasons, but may be revived on long term if resources become available. The ongoing upgrade of the ICRF antennas will depend on the success of the intermediate steps to reduce the tungsten sputtering. For a limited period starting in 2012, coverage of the limiters of 2 antennas with boron tiles is planned, to re-establish full operability of two ICRF systems with about 3 MW power. The final optimized antenna version may be integrated into the conducting wall around 2016.

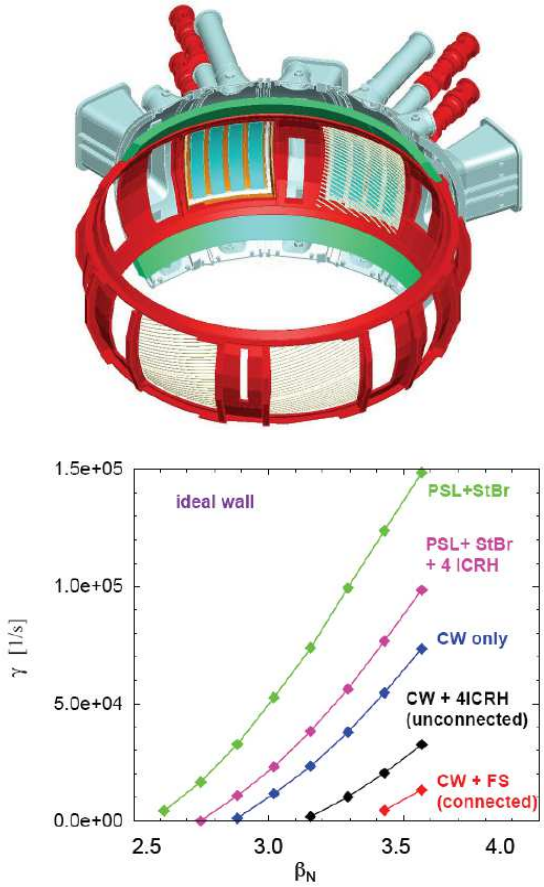

Fig. 15. Sketch of a posssible conducting wall design for ASDEX Upgrade, with 4 ICRF antennas integrated. The lower graph shows RWM growth rates for different wall coverage scenarios.

REFERENCES

[1] ASDEX Upgrade Team, guest Editor: A. Herrmann, *Special Issue on ASDEX Upgrade*. Fusion Science and Technology, Vol. 44, No. 3, 2003.

[2] R. Neu, M. Balden, V. Bobkov, R. Dux, O. Gruber, A. Herrmann, A. Kallenbach, M. Kaufmann, C. F. Maggi, H. Maier, H. W. Müller, T. Pütterich, R. Pugno, V. Rohde, A. C. C. Sips, J. Stober, W. Suttrop, C. Angioni, C. V. Atanasiu, W. Becker, K. Behler, K. Behringer, A. Bergmann, T. Bertoncelli, R. Bilato, A. Bottino, M. Brambilla, F. Braun, A. Buhler, A. Chankin, G. Conway, D. P. Coster, P. de Marné, S. Dietrich, K. Dimova, R. Drube, T. Eich, K. Engelhardt, H.-U. Fahrbach, U. Fantz, L. Fattorini, J. Fink, R. Fischer, A. Flaws, P. Franzen, J. C. Fuchs, K. Gál, M. García Muñoz, M. Gemisic-Adamov, L. Giannone, S. Gori, S. da Graca, H. Greuner, A. Gude, S. Günter, G. Haas, J. Harhausen, B. Heinemann, N. Hicks, J. Hobirk, D. Holtum, C. Hopf, L. Horton, M. Huart, V. Igochine, S. Kálvin, O. Kardaun, M. Kick, G. Kocsis, H. Kollotzek, C. Konz, K. Krieger, T. Kurki-Suonio, B. Kurzan, K. Lackner, P. T. Lang, P. Lauber, M. Laux, J. Likonen, L. Liu, A. Lohs, K. Mank, A. Manini, M.-E. Manso, M. Maraschek, P. Martin, Y. Martin, M. Mayer, P. McCarthy, K. McCormick, H. Meister, F. Meo, P. Merkel, R. Merkel, V. Mertens, F. Merz, H. Meyer, M. Mlynek, F. Monaco, H. Murmann, G. Neu, J. Neuhauser, B. Nold, J.-M. Noterdaeme, G. Pautasso, G. Pereverzev, E. Poli, M. Püschel, G. Raupp, M. Reich, B. Reiter, T. Ribeiro, R. Riedl, J. Roth, M. Rott, F. Ryter, W. Sandmann, J. Santos, K. Sassenberg, A. Scarabosio, G. Schall, J. Schirmer, A. Schmid, W. Schneider, G. Schramm, R. Schrittwieser, W. Schustereder, J. Schweinzer, S. Schweizer, B. Scott, U. Seidel, F. Serra, M. Sertoli, A. Sigalov, A. Silva, E. Speth, A. Stäbler, K.-H. Steuer, E. Strumberger, G. Tardini, C. Tichmann, W. Treutterer, C. Tröster, L. Urso, E. Vainonen-Ahlgren, P. Varela, L. Vermare, D. Wagner, M. Wischmeier, E. Wolfrum, E. Würsching, D. Yadikin, Q. Yu, D. Zasche, T. Zehetbauer, M. Zilker, and H. Zohm, "Plasma wall interaction and its implication in an all tungsten divertor tokamak," *Plasma Physics and Controlled Fusion*, vol. 49, no. 12B, pp. B59–B70, 2007. [Online]. Available: http://stacks.iop.org/0741-3335/49/B59

[3] A. Kallenbach, R. Neu, R. Dux, H.-U. Fahrbach, J. C. Fuchs,

L. Giannone, O. Gruber, A. Herrmann, P. T. Lang, B. Lipschultz, C. F. Maggi, J. Neuhauser, V. Philipps, T. Pütterich, V. Rohde, J. Roth, G. Sergienko, A. Sips, and ASDEX Upgrade Team, "Tokamak operation with high-z plasma facing components," *Plasma Physics and Controlled Fusion*, vol. 47, no. 12B, pp. B207–B222, 2005. [Online]. Available: http://stacks.iop.org/0741-3335/47/B207

[4] R. Neu, "Experience with high-z plasma facing materials and extrapolation to future devices," *IEEE Transactions on Plasma Science*, vol. 38, no. 3, pp. 453–460, jan 2010.

[5] A. Kallenbach, R. Dux, J. C. Fuchs, R. Fischer, B. Geiger, L. Giannone, A. Herrmann, T. Lunt, V. Mertens, R. McDermott, R. Neu, T. Pütterich, S. Rathgeber, V. Rohde, K. Schmid, J. Schweinzer, W. Treutterer, and ASDEX Upgrade Team, "Divertor power load feedback with nitrogen seeding in asdex upgrade," *Plasma Physics and Controlled Fusion*, vol. 52, no. 5, p. 055002, 2010. [Online]. Available: http://iopscience.iop.org/0741-3335/52/5/055002/

[6] R. Dux, A. Janzer, T. Pütterich, and ASDEX Upgrade Team, "Main chamber sources and edge transport of tungsten in h-mode plasmas at asdex upgrade," *Nuclear Fusion*, vol. 51, no. 5, p. 053002, 2011. [Online]. Available: http://stacks.iop.org/0029-5515/51/i=5/a=053002

[7] T. Pütterich, R. Dux, M. Janzer, R. McDermott, and ASDEX Upgrade Ream, "Elm flushing and impurity transport in the h-mode edge barrier in asdex upgrade," *Journal of Nuclear Materials*, vol. 415, no. 1, Supplement, pp. S334–S339, 2011. [Online]. Available: http://www.sciencedirect.com/science/article/B6TXN-516972H-1/2/df52f372e3587d9543c8542dd10c230c

[8] W. Suttrop, L. Barrera, A. Herrmann, R. M. McDermott, T. Eich, R. Fischer, B. Kurzan, P. T. Lang, A. Mlynek, T. Pütterich, S. K. Rathgeber, M. Rott, T. Vierle, E. Viezzer, M. Willensdorfer, E. Wolfrum, I. Zammuto, and ASDEX Upgrade Team, "Studies of edge localized mode mitigation with new active in-vessel saddle coils in asdex upgrade," *Plasma Physics and Controlled Fusion*, vol. 53, no. 12, p. 124014, 2011. [Online]. Available: http://stacks.iop.org/0741-3335/53/i=12/a=124014

[9] R. Neu, J. C. Fuchs, G. Haas, A. Herrmann, A. Kallenbach, M. Laux, J. Neuhauser, F. Ryter, J. Gafert, O. Gruber, M. Kaufmann, B. Kurzan, V. Mertens, H. W. Müller, V. Rohde, A. Sips, J. Stober, B. Streibl, W. Treutterer, and ASDEX Upgrade Team, "Properties of the new divertor IIb in ASDEX Upgrade," *Plasma Physics and Controlled Fusion*, vol. 44, no. 6, pp. 1021–1029, 2002. [Online]. Available: http://stacks.iop.org/0741-3335/44/1021

[10] A. Herrmann, H. Greuner, J. C. Fuchs, P. de Marne, R. Neu, and A. U. Team, "Experiences with tungsten coatings in high heat flux tests and under plasma load in asdex upgrade," *Physica Scripta*, vol. T138, p. 014059 (4pp), 2009. [Online]. Available: http://stacks.iop.org/1402-4896/T138/014059

[11] A. Herrmann, H. Greuner, N. Jaksic, B. Böswirth, H. Maier, R. Neu, S. Vorbrugg, and A. U. team, "A solid tungsten divertor for asdex upgrade," *PFMC 13 conference, accepted for publication in Physica Scripta*, 2011.

[12] A. Stäbler, J. Hobirk, F. Leuterer, F. Meo, and J.-M. Noterdaeme, "Current drive in ASDEX Upgrade," *Fusion Science and Technology*, vol. 44, no. 3, pp. 730–742, 2003. [Online]. Available: http://www.ans.org/pubs/journals/fst/vol/44-3-730-742.html

[13] S. Günter, G. Conway, S. da Graca, H.-U. Fahrbach, C. Forest, M. Garcia Munoz, T. Hauff, J. Hobirk, V. Igochine, F. Jenko, K. Lackner, P. Lauber, P. McCarthy, M. Maraschek, P. Martin, E. Poli, K. Sassenberg, E. Strumberger, G. Tardini, E. Wolfrum, H. Zohm, and ASDEX Upgrade Team, "Interaction of energetic particles with large and small scale instabilities," *Nuclear Fusion*, vol. 47, no. 8, pp. 920–928, 2007. [Online]. Available: http://stacks.iop.org/0029-5515/47/920

[14] B. Geiger, M. Garcia-Munoz, W. W. Heidbrink, R. M. McDermott, G. Tardini, R. Dux, R. Fischer, V. Igochine, and ASDEX Upgrade Team, "Fast-ion d-alpha measurements at asdex upgrade," *Plasma Physics and Controlled Fusion*, vol. 53, no. 6, p. 065010, 2011. [Online]. Available: http://stacks.iop.org/0741-3335/53/i=6/a=065010

[15] V. Bobkov, F. Braun, R. Dux, L. Giannone, A. Herrmann, A. Kallenbach, H. W. Müller, R. Neu, J.-M. Noterdaeme, T. Pütterich, V. Rohde, and ASDEX Upgrade Team, "Operation of icrf antennas in a full tungsten environment in ASDEX Upgrade," *Journal of Nuclear Materials*, vol. 390-391, pp. 900–903, 2009. [Online]. Available: http://www.sciencedirect.com/science/article/B6TXN-4VG7MW6-6/2/27a0612887675b7741345c5a487833d1

[16] V. Bobkov, F. Braun, R. Dux, A. Herrmann, L. Giannone, A. Kallenbach, A. Krivska, H. Müller, R. Neu, J.-M. Noterdaeme, T. Pütterich, V. Rohde, J. Schweinzer, A. Sips, I. Zammuto, and A. U. Team, "Assessment of compatibility of icrf antenna operation with full w wall in asdex upgrade," *Nuclear Fusion*, vol. 50, no. 3, p. 035004 (11pp), 2010. [Online]. Available: http://www.iop.org/EJ/abstract/0029-5515/50/3/035004

[17] R. M. McDermott, C. Angioni, R. Dux, A. Gude, T. Pütterich, F. Ryter, G. Tardini, and ASDEX Upgrade Team, "Effect of electron cyclotron resonance heating (ecrh) on toroidal rotation in asdex upgrade h-mode discharges," *Plasma Physics and Controlled Fusion*, vol. 53, no. 3, p. 035007, 2011. [Online]. Available: http://stacks.iop.org/0741-3335/53/i=3/a=035007

[18] C. Angioni, R. McDermott, E. Fable, R. Fischer, T. Pütterich, F. Ryter, G. Tardini, and ASDEX Upgrade Team, "Gyrokinetic modelling of electron and boron density profiles of h-mode plasmas in asdex upgrade," *Nuclear Fusion*, vol. 51, no. 2, p. 023006, 2011. [Online]. Available: http://stacks.iop.org/0029-5515/51/i=2/a=023006

[19] R. M. McDermott, C. Angioni, R. Dux, E. Fable, T. Pütterich, F. Ryter, A. Salmi, T. Tala, G. Tardini, E. Viezzer, and ASDEX Upgrade Team, "Core momentum and particle transport studies in the asdex upgrade tokamak," *Plasma Physics and Controlled Fusion*, vol. 53, no. 12, p. 124013, 2011. [Online]. Available: http://stacks.iop.org/0741-3335/53/i=12/a=124013

[20] A. Mlynek, M. Reich, L. Giannone, W. Treutterer, K. Behler, H. Blank, A. Buhler, R. Cole, H. Eixenberger, R. Fischer, A. Lohs, K. Lüddecke, R. Merkel, G. Neu, F. Ryter, D. Zasche, and ASDEX Upgrade Team, "Real-time feedback control of the plasma density profile on asdex upgrade," *Nuclear Fusion*, vol. 51, no. 4, p. 043002, 2011. [Online]. Available: http://stacks.iop.org/0029-5515/51/i=4/a=043002

[21] J. E. Rice, A. Ince-Cushman, M. L. Reinke, Y. Podpaly, M. J. Greenwald, B. LaBombard, and E. S. Marmar, "Spontaneous core toroidal rotation in alcator c-mod l-mode, h-mode and itb plasmas," *Plasma Physics and Controlled Fusion*, vol. 50, p. 124042, 2008.

[22] M. Reich, K. Behler, R. Drube, L. Giannone, A. Kallenbach, A. Mlynek, J. Stober, W. Treutterer, and ASDEX Upgrade team, "Real-time diagnostics and their applications at ASDEX Upgrade," *Fusion Science and Technology*, vol. 58, no. 3, p. 727, 2010. [Online]. Available: http://epubs.ans.org/?a=10921

[23] T. E. Evans, R. A. Moyer, J. G. Watkins, T. H. Osborne, P. R. Thomas, M. Becoulet, J. A. Boedo, E. J. Doyle, M. E. Fenstermacher, K. H. Finken, R. J. Groebner, M. Groth, J. H. Harris, G. L. Jackson, R. J. La Haye, C. J. Lasnier, S. Masuzaki, N. Ohyabu, D. G. Pretty, H. Reimerdes, T. L. Rhodes, D. L. Rudakov, M. J. Schaffer, M. R. Wade, G. Wang, W. P. West, and L. Zeng, "Suppression of large edge localized modes with edge resonant magnetic fields in high confinement DIII-D plasmas," *Nuclear Fusion*, vol. 45, no. 7, pp. 595–607, 2005.

[24] Y. Liang, H. Koslowski, P. Thomas, E. Nardon, S. Jachmich, A. Alfier, G. Arnoux, Y. Baranov, M. Becoulet, M. Beurskens, R. Coelho, T. Eich, E. D. L. Luna, W. Fundamenski, S. Gerasimov, C. Giroud, M. Gryaznevich, D. Harting, A. Huber, A. Kreter, L. Moreira, V. Parail, S. Pinches, S. Saarelma, O. Schmitz, and JET-EFDA contributors, "Active control of type-i edge localized modes with n = 1 and n = 2 fields on jet," *Nuclear Fusion*, vol. 50, no. 2, p. 025013, 2010. [Online]. Available: http://stacks.iop.org/0029-5515/50/i=2/a=025013

[25] H. Zohm, "On the minimum size of demo," *Fusion Science and Technology*, vol. 58, pp. 613–624, 2010.

[26] R. Neu, J. Fuchs, A. Kallenbach, R. Dux, T. Eich, R. Fischer, O. Gruber, A. Herrmann, A. Janzer, H. Müller, T. Pütterich, J. Rapp, V. Rohde, K. Schmid, J. Schweinzer, M. Sertoli, G. Rooij, and ASDEX Upgrade Team, "Power and particle exhaust control in all w asdex upgrade," in *Proc. of the 23rd IAEA Fusion Energy Conference, Daejon, Korea Rep. of*, vol. IAEA-CN-180. Vienna: IAEA, 2010, pp. EXD/P3–24. [Online]. Available: http://www-pub.iaea.org/mtcd/meetings/PDFplus/2010/cn180/cn180_papers/EXD_P3-24.pdf

PLACE
PHOTO
HERE

Arne Kallenbach was born on May 9, 1959 in Hannover, Germany. He received the Diplom Physiker degree and Dr. rer. nat. degree from the University of Hannover, Hannover, Germany, in 1984 and 1988, respectively. After the habilitation in physics in 1995, he became a private lecturer with the universities of Hannover and Augsburg. In 2002, he was awarded the title Extra-ordinary Professor at the University of Hannover. Since 1988, he is Scientific employee at the Max-Planck-Institu für Plasmaphysik in Garching, Germany, doing spectroscopic studies at the ASDEX tokamak. In 1992, he became session leader at the ASDEX Upgrade tokamak, from 1995 till 2006 he was the group leader for spectroscopy. From 2001-2002, he was deputy task force leader for exhaust physics at JET. From 2007-2010, he was acting division head responsible for edge physics at ASDEX Upgrade, in 2010 he became the Leader of the ASDEX Upgrade Project. Prof. Kallenbach has been a member of the German Physical Society since 1984 and a member of its advisory board for plasma physics from 1998-2000.